JOURNAL OF GEOPHYSICAL RESEARCH, VOL. 105, NO. E8, PAGES 20,263–20,273, AUGUST 25, 2000

Sensitivity studies of methane photolysis and its impact on hydrocarbon chemistry in the atmosphere of Titan

Eric H. Wilson and Sushil K. Atreya

Department of Atmospheric, Oceanic, and Space Sciences, University of Michigan, Ann Arbor

Abstract. The photodissociation of methane at Lyman α (1216 Å) has been the focus of much scrutiny over the past few years. Methane photolysis leads to the formation of H_2 molecules as well as H, CH, $^1CH_2$, $^3CH_2$, and CH_3 radicals, which promote the propagation of hydrocarbon chemistry. However, recent studies [*Mordaunt et al.*, 1993; *Romani*, 1996; *Smith and Raulin*, 1999] have not fully resolved the issue of methane photolytic product yields at this wavelength. We use a one-dimensional photochemical model with updated chemistry to investigate the significance of these quantum yield schemes on the hydrocarbon chemistry of Titan's atmosphere, where Lyman α radiation accounts for 75% of methane photolysis longward of 1000 Å. Sensitivity studies show that while simple hydrocarbons like C_2H_2 (acetylene) and C_2H_4 (ethylene), which serve as important intermediates to the formation of more complex hydrocarbons, show virtually no variation in abundance, minor C_3 molecules do show substantial sensitivity to choice of quantum yield scheme. We find that the C_3H_4 isomers (methylacetylene, allene) and C_3H_6 (propylene) display major variation in atmospheric mixing ratios under the implementation of these schemes, with a maximum variation of approximately a factor of 5 in C_3H_4 abundance and approximately a factor of 4 for C_3H_6. In these cases our nominal scheme, recommended by *Romani* [1996], offers an intermediate result in comparison with the other schemes. We also find that choice of pathway for non-Lyman α methane absorption does affect hydrocarbon chemistry in the atmosphere of Titan, but this effect is minimal. A 65% variation in C_2H_6 (ethane) abundance, a value within observational uncertainty, is the largest divergence found for a wide range of possible non-Lyman α photofragment quantum yields. These results will have significance in future modeling and interpretation of observations of the atmosphere of Titan.

1. Introduction

Methane is the most important chemically active species in the upper atmosphere of Titan. At Lyman α the photodissociation of methane is capable of producing methyl radicals (CH_3), excited- and ground-state methylene radicals ($^1CH_2$, $^3CH_2$), methylidyne radicals (CH), and atomic and molecular hydrogen (H, H_2) through five spin-conserved and energetically allowed pathways [*Mordaunt et al.*, 1993]:

(J1) $CH_4 + h\nu \rightarrow CH_3 + H$ ($\lambda \leq 2742$ Å)

(J2) $\rightarrow {}^1CH_2 + H_2$ ($\lambda \leq 2443$ Å)

(J3) $\rightarrow {}^1CH_2 + 2H$ ($\lambda \leq 1294$ Å)

(J4) $\rightarrow {}^3CH_2 + 2H$ ($\lambda \leq 1340$ Å)

(J5) $\rightarrow CH + H_2 + H$. ($\lambda \leq 1355$ Å)

The threshold wavelengths are determined from heats of formation at 200 K and established electronic levels for methylene [*Chase et al.*, 1985]. Methane has a significant absorption cross section at wavelengths shorter than 1450 Å [*Mount et al.*, 1977; *Mount and Moos*, 1978; *Lee and Chiang*, 1983], and coupled with the solar UV flux spectrum, ~75% of its absorption of radiation longward of 1000 Å is due to the intense solar flux at Lyman α (1216 Å), as shown in Figure 1. Lyman α absorption peaks near 750 km at the Lyman α unit optical depth for CH_4 absorption, and the solar Lyman α emission is completely extinguished below 625 km.

Methane photodissociation provides the basis for the production of various hydrocarbons, many of which have been observed [*Coustenis et al.*, 1989, 1991; *Coustenis and Bézard*, 1995; *Kostiuk et al.*, 1997] in the stratosphere, with methane itself and acetylene having been observed in the thermosphere [*Smith et al.*, 1982] . The formation, as well as the condensation and polymerization of these hydrocarbons within a background N_2 atmosphere, creates a diverse environment in which organic chemistry can flourish. From this structure of organic chemistry are presented some key rate coefficients and cross-section references in Table 1. This organic chemistry may be similar to that which characterized the primitive, prebiotic Earth [*Raulin et al.*, 1998], making Titan a compelling study for researchers of many different disciplines.

The pathways of methane photochemistry are influenced by the background gas in which methane resides. In Jovian atmospheres the initiation of methane photochemistry takes on a different look. Ground-state methylene radicals are converted to methylidyne radicals (R1), while excited methylene and methylidyne radicals at high pressures are quickly converted to methyl radicals [*Langford et al.*, 1983; *Brownsword et al.*, 1997a]. Also, a substantial amount of CH formed results in the production of C_2H_2 via (R4) and (J6) [*Romani et al.*, 1993]. On the other hand, in Titan's atmosphere the preeminence of N_2, rather than H_2, provides different primary pathways for CH and $^1CH_2$ from those in Jovian atmospheres. A nitrogen atmosphere

Paper number 1999JE001221.
0148-0227/00/1999JE001221$09.00

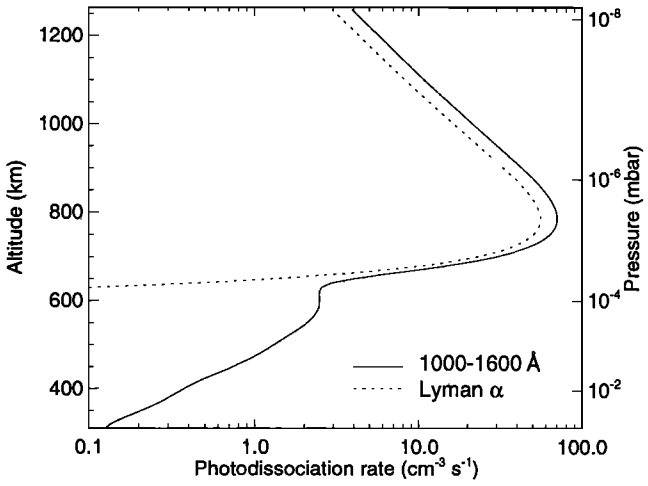

Figure 1. Methane photodissociation rates from solar radiation absorbed at 1000-1600 Å (solid line) and at Lyman α (dotted line).

offers fewer significant mechanisms for the conversion of $^1CH_2$ to CH_3, and thus collisional quenching of excited methylene plays a more prominent role. This process directs more methane into the formation of C_2H_2 as opposed to C_2H_6, and thus we expect to find a much lower C_2H_6/C_2H_2 ratio in the atmosphere of Titan than in the Jovian atmosphere. However, because of the complexities involved in these methane photochemical schemes, the photolysis of methane must be treated with precision.

There have been a few recent studies [*Mordaunt et al.*, 1993; *Romani*, 1996; *Heck et al.*, 1996; *Brownsword et al.*, 1997b; *Smith and Raulin*, 1999] that have centered on determining product quantum yields of methane photolysis only at Lyman α, yielding contradictory results. In this work we will evaluate these studies and determine what effect pathway branching ratios have on the subsequent chemistry of Titan's atmosphere. In addition, an examination of methane photolysis quantum yields outside of Lyman α will seek to reveal the significance of methane absorption at these wavelengths concerning the atmosphere of Titan.

2. Methane Product Quantum Yields

Many collisional photolysis studies of methane dissociation involving end-product analyses [*Mahan and Mandal*, 1962; *Magee*, 1963; *Ausloos et al.*, 1964; *Braun et al.*, 1966] have been conducted; however, the highly reactive nature of CH_x (x=1, 2, 3) radicals has called the reliability of these studies into question owing to possible secondary reactions. *Laufer and McNesby* [1968], using a split-cell collisional photolysis technique, measured the total H and H_2 quantum yields at 0.42 and 0.59, respectively, at 1236 Å. *Rebbert and Ausloos* [1972/1973] measured $C(^1D)$ and CH quantum yields from methane photolysis by rare gas resonance lamps at 1048-1067 Å and 1236 Å. Their end-product analysis revealed a $C(^1D)$ quantum yield of $6.5x10^{-3}$ at 1048-1067 Å and $4x10^{-3}$ at 1236 Å and a CH quantum yield of 0.23 at 1048-1067 Å and 0.06 at 1236 Å, indicating the lack of significance of a $C(^1D)$ pathway. Assuming a monotonically decreasing yield for CH renders a yield of 0.08 at Lyman α.

More recently, collision-free studies of primary product quantum yields have been conducted at Lyman α. *Slanger and Black* [1982] used noncollisional resonance fluorescence to measure the H atom yield at 1216 Å. Their cumulative quantum yield value of 1.16 contradicts the earlier measurements of *Laufer and McNesby* [1968], suggesting that the previous low measured yield may have been due to the high reactivity of atomic hydrogen in their collisional studies. Assuming the Laufer and McNesby 1236 Å value for H_2 to be valid at Lyman α and an interpolated CH quantum yield of 0.08 [*Rebbert and Ausloos*, 1972/1973], Slanger and Black adopted a value for (J2) of 0.47 and discarded (J1) as being of negligible importance in the photodissociation of methane. The *Yung et al.* [1984] Titan model, using the *Rebbert and Ausloos* [1972/1973] result and aided by the earlier work of *Strobel* [1973] and the measurements of *Slanger and Black* [1982], adopted a scheme dominated by CH_2 production with a conspicuous absence of CH_3 formation.

Mordaunt et al. [1993] provided the first direct measurement of methyl radical production through H atom photofragment translational spectroscopy, tracking the kinetic energies of H photofragments from Rydberg time-of-flight data. Noting that CH_3 will accompany "fast" H atoms while "slow" H atoms would be distributed through pathways (J3) - (J5), Mordaunt et al. determine the probable CH_3 quantum yield to be ~0.5. These measurements, however, were not able to constrain the other photolytic pathways. Nevertheless, the analysis of Mordaunt et al. based on Rice-Ramsperger-Kassel-Marcus (RRKM) theory does provide some insight into the outcome of the methyl vibrationally excited metastable fragment, denoted as $CH_3^{\neq}$, the intermediate between the photon absorption process and the products thereof, created by the initial C-H bond fission process. Through this examination, Mordaunt et al. offer a theoretical basis for the distribution of yields for pathways (J2) - (J5). This is presented in the form of two separate schemes describing the quantum yields of the pathways of methane photolysis, which are shown in Table 2, both of which present scenarios that contradict previous measurements. The most striking contradiction is the yield of CH_3, which is indicated to be a significant pathway in the Lyman α photolysis of methane, contrary to what was assumed from previous studies [*Mahan and Mandal*, 1962; *Magee*, 1963; *Braun et al.*, 1966; *Laufer and McNesby*, 1968; *Rebbert and Ausloos*, 1972/1973; *Slanger and Black*, 1982]. Furthermore, a Doppler-selected time-of-flight study by *Wang and Liu* [1998] verifies the significance of the (J1) pathway, indicating the ratio of (J1) to (J3)-(J5) at 3:1. The total H atom quantum yield for both Mordaunt et al. models is 1.0, which stands in good agreement with the value from *Slanger and Black* [1982]. However, the high CH yield of scheme 2 has not been corroborated by further study, before or since, and thus is not likely. The authors caution that the two schemes presented are limiting cases, and the actual yield distribution probably falls somewhere in between.

Romani [1996] in his investigation of the ethane/acetylene ratio on Jupiter attempted to determine the branching ratios, adhering to constraints provided by previous measurements [*Laufer and McNesby*, 1968; *Rebbert and Ausloos*, 1972/1973; *Slanger and Black*, 1982; *Mordaunt et al.*, 1993]. Although the sum of these measurements provides numerous contradictions, Romani conducted a least squares calculation using those constraints provided, presenting a scheme that agrees most directly with previous studies. This best fit scheme, with (J3) set equal to zero, is also presented in Table 2. This scheme provides good agreement for the CH quantum yield with *Rebbert and Ausloos* [1972/1973] and decent agreement for the H and CH_3 quantum yields with *Mordaunt et al.* [1993]. The Romani scheme at Lyman α provides the scheme most consistent with

Table 1. Rate Coefficients of Some Important Reactions and References for Some Key Cross Sections Adopted in Our Model

Reactions	Rate coefficients	References
(R1) $^3CH_2 + H \rightarrow CH + H_2$	$4.7\times10^{-10}e^{-370/T}$	*Zabarnick et al.* [1986]
(R2) $^1CH_2 + CH_4 \rightarrow 2CH_3$	6.0×10^{-11}	*Bohland et al.* [1985]
(R3) $^3CH_2 + CH_3 \rightarrow C_2H_4 + H$	7.0×10^{-11}	*Tsang and Hampson* [1986]
(R4) $CH + CH_4 \rightarrow C_2H_4 + H$	$3.96\times10^{-8}T^{1.04}e^{-36.1/T}$	*Canosa et al.* [1997]
(R5) $C_2H + CH_4 \rightarrow C_2H_2 + CH_3$	$1.2\times10^{-11}e^{-491/T}$	*Opansky and Leone* [1996]
(R6) $^1CH_2 + N_2 \rightarrow ^3CH_2 + N_2$	$2.36\times10^{-14}T$	*Wagener* [1990]
(R7) $C_2H + C_2H_2 \rightarrow C_4H_2 + H$	$9.53\times10^{-11}e^{30.8/T}$	*Chastaing et al.* [1998]
(R8) $C_2H_2 + H \xrightarrow{M} C_2H_3$	$k_0=3.3\times10^{-30}e^{-740/T}$ $k_\infty=1.4\times10^{-11}e^{-1300/T}$	*Baulch et al.* [1992]
(R9) $C_2H_3 + H \xrightarrow{M} C_2H_4$	$k_0=5.76\times10^{-24}T^{-1.3}$ $k_\infty=8.0\times10^{-11}$	*Monks et al.* [1995]
(R10) $CH_3 + CH_3 \xrightarrow{M} C_2H_6$	$k_0=8.76\times10^{-7}T^{-7.03}e^{-1390/T}$ $k_\infty=1.5\times10^{-7}T^{-1.18}e^{-329/T}$ $F_c=0.381e^{-T/73.2}-0.619e^{-T/1180}$	*Slagle et al.* [1988]
(R11) $CH + C_2H_6 \rightarrow C_3H_6 + H$	$1.9\times10^{-8}T^{0.859}e^{-53.2/T}$	*Canosa et al.* [1997]
(R12) $CH + C_2H_4 \rightarrow CH_3C_2H + H$	$3.87\times10^{-9}T^{0.546}e^{-29.6/T}$	*Canosa et al.* [1997]
(R13) $CH + C_2H_4 \rightarrow CH_2CCH_2 + H$	$3.87\times10^{-9}T^{0.546}e^{-29.6/T}$	*Canosa et al.* [1997]
(R14) $CH_2CCH_2 + H \xrightarrow{M} CH_3C_2H + H$	$1.29\times10^{-11}e^{-1156/T}$	*Aleksandrov et al.* [1980]
(J1)-(J5) $CH_4 + h\nu \rightarrow$		*Mount et al.* [1977]; *Mount and Moos* [1978]
(J6) $C_2H_4 + h\nu \rightarrow$		*Chang et al.* [1998]
(J7) $C_2H_2 + h\nu \rightarrow$		*Okabe* [1981, 1983]; *Seki and Okabe* [1993]

Three-body reactions are calculated according to the expression $k=k_0k_\infty M/(k_0M+k_\infty)$ or, if F is given, $k=k_0k_\infty MF/(k_0M+k_\infty)$

previous measurements adopted for this wavelength [*Laufer and McNesby*, 1968; *Rebbert and Ausloos*, 1972/1973; *Slanger and Black*, 1982; *Mordaunt et al.*, 1993]. This scheme has been used in photochemical models of the Jovian planets [*Romani*, 1996; *Edgington et al.*, 1998; *Bishop et al.*, 1998] and is our nominal scheme for methane Lyman α absorption in the atmosphere of Titan.

The importance of pathway (J1) has been further corroborated by the study of *Heck et al.* [1996], which used photofragment ion imaging to obtain the speed and angular distribution of H atom photofragments, confirming the findings of *Mordaunt et al.* [1993] that H and H_2 photofragments are formed via a fast channel and a slow channel. Heck et al. propose that the H atom fast channel products of (J1) are dominant over the products of the slow channel of (J3) and (J5) by a 6:1 ratio, although they leave open the possibility of further decomposition of the $CH_3^{\neq}$ intermediate fragment into pathways (J3) and (J5). They also substantiate the assertion of *Romani* [1996] that (J2) is the primary channel of H_2 photofragment production through analysis of the fast and slow channel distributions.

However, the H atom quantum yield asserted by *Romani* [1996] and *Mordaunt et al.* [1993] has recently been brought into question by *Brownsword et al.* [1997b] through their laser photolysis and induced fluorescence technique. Using the H atom signal from H_2O photolysis as calibration, Brownsword et al. determine an H atom quantum yield of 0.47±0.11, which falls into agreement with the earlier work of *Laufer and McNesby* [1968] but is contrary to the results of *Slanger and Black* [1982] and *Mordaunt et al.* [1993]. The authors point out that the results of Mordaunt et al. were determined using HCN photolysis in a calibration method for H atom production. This technique, according to Brownsword et al., resulted in large uncertainties in

Table 2. Lyman α Methane Photolysis Quantum Yields

Pathways	*Mordaunt et al.* [1993]		*Romani* [1996]	*Smith and Raulin* [1999]
	Model 1 (MOR1)	Model 2 (MOR2)	(nominal)	(SR)
(J1) $CH_4 + h\nu \rightarrow CH_3 + H$	0.51	0.49	0 41	0.41
(J2) $CH_4 + h\nu \rightarrow {}^1CH_2 + H_2$	0.24	0.00	0.28	0.53
(J3) $CH_4 + h\nu \rightarrow {}^1CH_2 + 2H$	0.00	0.00	0.00	0 00
(J4) $CH_4 + h\nu \rightarrow {}^3CH_2 + 2H$	0.25	0.00	0.21	0.00
(J5) $CH_4 + h\nu \rightarrow CH + H_2 + H$	0.00	0 51	0.10	0.06

the H atom quantum yield for Lyman α methane photolysis owing to the low temperatures of the jet-cooled sample and the lack of available data concerning HCN and CH_4 absorption at these low temperatures. *Smith and Raulin* [1999] offer a scheme for methane photodissociation, shown in Table 2, based on the recent measurements of *Heck et al.* [1996] and *Brownsword et al.* [1997b], in which the production of atomic hydrogen is sharply reduced and the formation of the ground-state methylene radical is eliminated.

Study of methane photolysis at wavelengths other than Lyman α in recent years has been nonexistent. Collisional energetics show that only (J1) and (J2) are energetically possible throughout the domain of methane absorption. The lack of research in this area has encouraged modelers to assume a unit quantum yield for one of the energetically allowed pathways for the sake of simplification. Collisional studies conducted at 1236 Å [*Mahan and Mandal*, 1962; *Ausloos et al.*, 1964] and at 1048-1067 Å [*Magee*, 1963] suggested that CH_2 was the primary product of methane photodissociation. However, the possibility of the corruption of these results from secondary reactions along with the emergence of CH_3 in recent Lyman α studies suggest otherwise. With this in mind, we adopt (J1) as the nominal pathway for wavelengths other than Lyman α.

3. Sensitivity Studies

To determine the impact of methane photolysis quantum yields on abundance profiles, we use a one-dimensional, steady state, globally averaged, photochemical model that extends from Titan's surface to 1265 km. This model solves the steady state continuity equation

$$P_i - L_i = \frac{1}{r^2}\frac{\partial\left(r^2\Phi_i\right)}{\partial r}, \qquad (1)$$

where P_i is the production rate of species i, L_i is the loss rate, the radius $r = (R_0+z)$, where R_0 is the radius of Titan and z is the altitude, and Φ_i is the vertical flux, which can be expressed as

$$\Phi_i(z) = -D_i\left[n\frac{\partial\xi_i}{\partial z} + \xi_i\frac{\partial n}{\partial z} + (1+\alpha_i)\frac{n\xi_i}{T}\frac{\partial T}{\partial z} + \frac{n\xi_i}{H_i}\right] - Kn\frac{\partial\xi_i}{\partial z}, \qquad (2)$$

where n is the total number density, ξ_i is the mixing ratio, D_i is the molecular diffusion coefficient, K is the eddy diffusion coefficient, H_i is the scale height, α_i is the thermal diffusion coefficient, and T is the temperature. The chemistry of this model is based on the *Toublanc et al.* [1995] model, with the inclusion of CH and relevant reactions, and updated chemical rate coefficients and cross sections appropriate for the atmospheric conditions of Titan. This model calculates mixing ratios for 61 species, including hydrocarbons, oxygen compounds, and nitriles, taking into account the absorption and N_2-Rayleigh scattering of UV photons from 1000 to 3000 Å. Our thermal and eddy diffusion profile is shown in Figure 2.

3.1. Lyman α

We present comparisons of mixing ratio and production rate profile with the four schemes described in Table 2 at Lyman α, using our nominal scheme of a CH_3 unit quantum yield at all other wavelengths for sake of comparison. The four schemes will hereafter be referred to as the following: *Mordaunt et al.* [1993] schemes 1 and 2, MOR1 and MOR2; *Romani* [1996] scheme, nominal; *Smith and Raulin* [1999] scheme, SR. The MOR1 scheme was adopted in the *Toublanc et al.* [1995] model, while the MOR2 scheme was adopted in the *Lara et al.* [1996] model of Titan's atmosphere. The main source of the photofragments in Titan's upper atmosphere (> 600 km) is methane photolysis, demonstrated by the fact that the peak of production of the photofragments in the upper atmosphere corresponds with the peak of methane photolysis at ~750 km (Figures 1, 3, and 4). In the lower atmosphere the peaks for $^1CH_2$ and $^3CH_2$ (Figure 3) are due to photolysis of higher-order hydrocarbons, while the H peak (Figure 4c) is due mainly to direct acetylene photolysis and the CH_3 peak (Figure 4b) is due indirectly to acetylene photolysis and recycling by the scheme

$$\begin{aligned} C_2H_2 + h\nu &\rightarrow C_2H + H \\ C_2H + CH_4 &\rightarrow C_2H_2 + CH_3 \\ \hline CH_4 &\rightarrow CH_3 + H \end{aligned} \qquad (S1)$$

In fact, acetylene photolysis accounts for ~75% of the atomic hydrogen formed below 600 km, while this catalytic dissociation of methane via C_2H is responsible for 67% of CH_3 produced below 600 km.

Excited metastable methylene, $^1CH_2$, is produced in greater quantities by SR, 65% more than the nominal scheme's production of 4.02×10^8 cm^{-2} s^{-1} above 600 km (Figure 3a). Owing to the absence of methylene production via methane

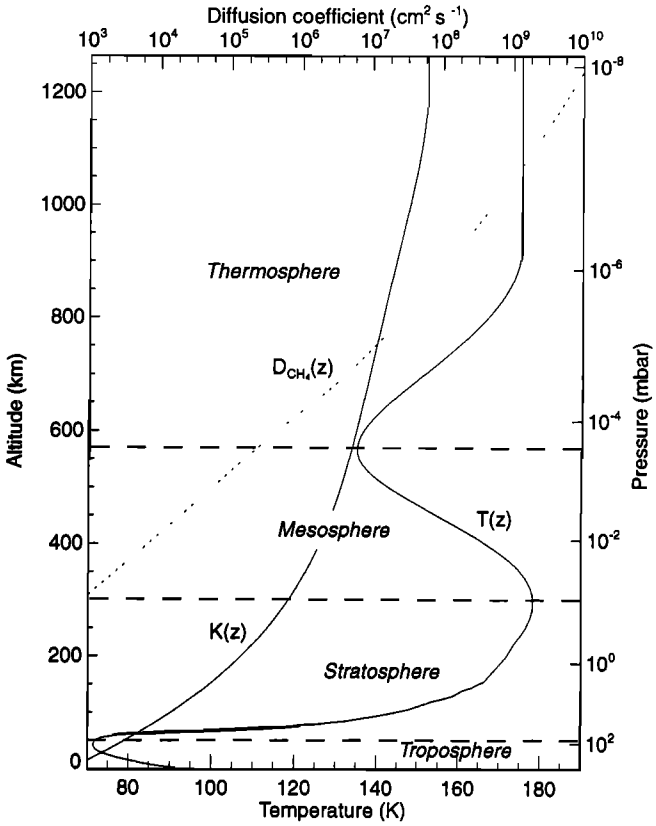

Figure 2. Temperature and diffusion profiles for the atmosphere of Titan. K(z) denotes the eddy diffusion profile used in this study, while $D_{CH_4}(z)$ represents the methane molecular diffusion profile. Temperatures from 0 to 200 km were obtained from Voyager 1 occultation measurements by *Lindal et al.* [1983] while temperatures from 200 to 1265 km were obtained from the recommended engineering model of *Yelle et al.* [1997].

photolysis, the MOR2 $^1CH_2$ production rate profile, which yields about 2.5 times less $^1CH_2$ than the nominal scheme in the upper atmosphere, is controlled by the less effective process of CH_3 photolysis, responsible for over 95% of the thermospheric $^1CH_2$ created by the MOR2 scheme. The profiles converge below ~625 km, where the influence of Lyman α methane photolysis is eliminated. This profile behavior influences the production of the ground-state methylene molecule, $^3CH_2$. This radical is produced through both direct methane dissociation (J4) (43% of $^3CH_2$ above 600 km) and $^1CH_2$ quenching (51% of $^3CH_2$ above 600 km):

$$CH_4 + h\nu \rightarrow {}^3CH_2 + 2H$$

$$\begin{aligned} CH_4 + h\nu &\rightarrow {}^1CH_2 + H_2 \\ {}^1CH_2 + N_2 &\rightarrow {}^3CH_2 + N_2 \\ \hline CH_4 &\rightarrow {}^3CH_2 + H_2 \end{aligned} \quad \text{(S2)}$$

Although the SR scheme does not permit any direct Lyman α production of $^3CH_2$, the SR production rate of $^3CH_2$ due to quenching is approximately equal to the nominal and MOR1 production of $^3CH_2$ from photolysis and quenching at the peak of CH_4 photolysis (Figure 3b). The similarity of the total methylene yields of the three schemes at Lyman α is responsible for this fact, as much of the $^1CH_2$ produced is quenched to the ground state. With the SR scheme's reliance on $^1CH_2$ quenching for $^3CH_2$ production and the characteristic drop in quenching rate with increasing altitude as a result of decreasing N_2 density, $^3CH_2$ production for SR clearly drops with respect to the nominal and MOR1 schemes near the top of the model.

The CH production rate is largely dependent on methane photolysis at Lyman α, both directly (J5) and through reaction of the photofragments $^3CH_2$ and H:

$$^3CH_2 + H \rightarrow CH + H_2 . \quad \text{(R1)}$$

(R1) produces CH molecules at a rate of 1.5×10^8 cm^{-2} s^{-1} above 600 km for the nominal case, accounting for 62% of CH molecules produced in this region of the atmosphere. With its dependence on Lyman α radiation, the CH production rate falls off below 600 km, as shown in Figure 4a. The higher nominal yield of CH results in 40-65% larger CH column production in the thermosphere, compared to SR and MOR1. However, the even larger CH yield of MOR2 translates into a column production rate ~110% larger than the nominal rate. The MOR2 profile is not as affected by the decreased influence of $^1CH_2$ quenching higher in the atmosphere via (R1), as there is no $^1CH_2$ production from Lyman α methane photolysis in the MOR2 scheme. As a result, MOR2 shows an increasing ratio to the other rates with increasing altitude for CH. Therefore CH plays a larger role in the chemistry of the upper atmosphere under the MOR2 scheme than in the other schemes.

CH_3 production in the upper atmosphere is governed mainly by direct methane photolysis and conversion from $^1CH_2$ radicals:

$$^1CH_2 + CH_4 \rightarrow 2CH_3 . \quad \text{(R2)}$$

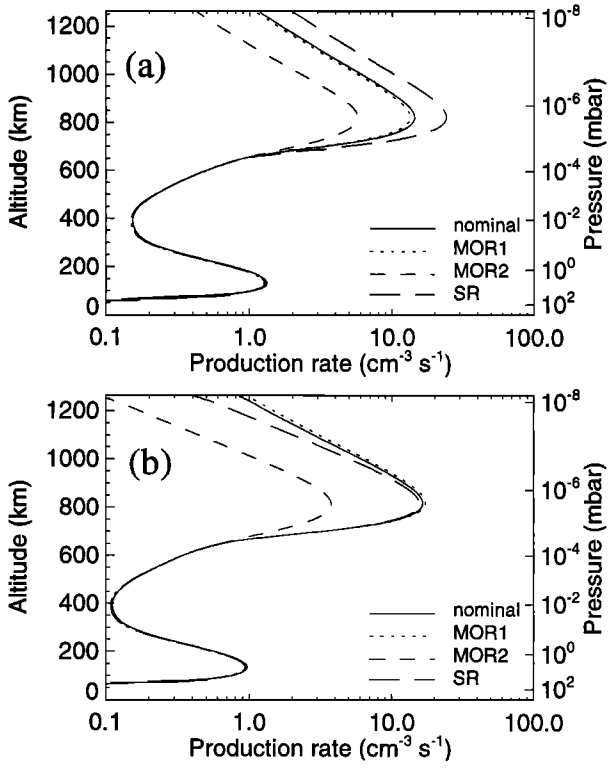

Figure 3. (a) The $^1CH_2$ production rate from the Lyman α-varying schemes. (b) The $^3CH_2$ production rate from the Lyman α-varying schemes due solely to methane photolysis and quenching of $^1CH_2$. The solid line denotes the production rates for the nominal case, the dotted line denotes MOR1, the short-dashed line denotes MOR2, and the long-dashed line denotes SR.

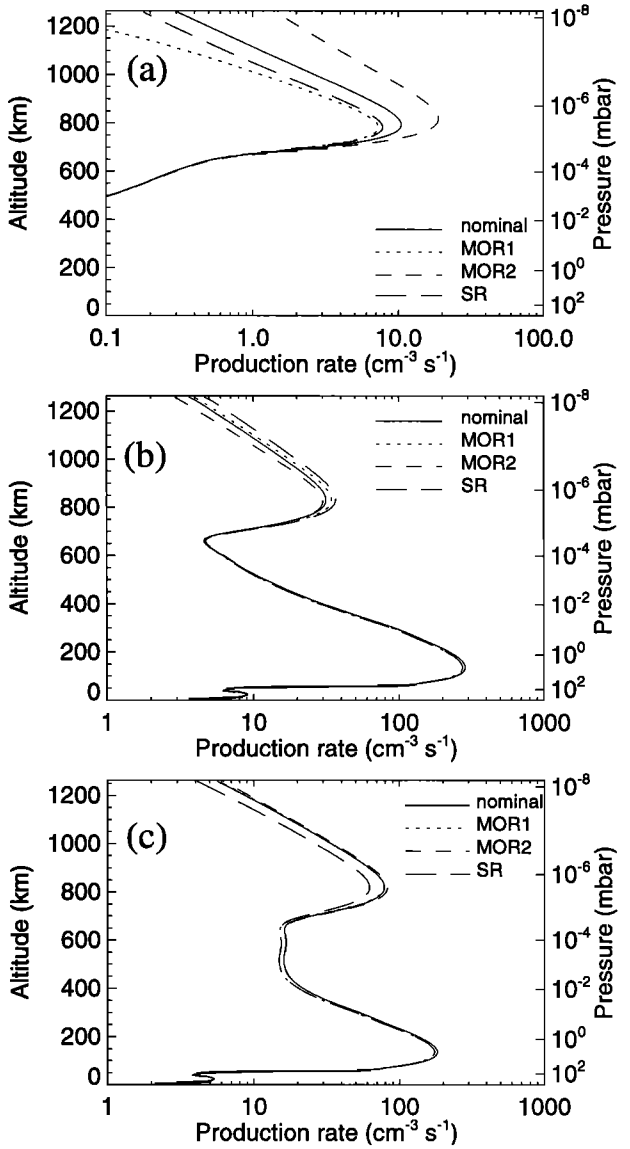

Figure 4. Production rates from the Lyman α-varying schemes for the following constituents: (a) CH, (b) CH_3, and (c) H.

This process is responsible for the loss of 1.49×10^8 cm^{-2} s^{-1} $^1CH_2$ molecules in the thermosphere. In fact, methane conversion accounts for 30% of CH_3 created in the thermosphere, while methane photolysis accounts for 67%, in the nominal scheme. Thus, although the MOR1 and MOR2 schemes assume the largest direct methyl radical yield of the four schemes, methane conversion through $^1CH_2$ insertion provides a significant source of CH_3 radicals. In fact, SR with its large $^1CH_2$ yield produces the most CH_3, and MOR2 with no $^1CH_2$ yield produces the least (Figure 4b). However, the profiles do not vary much among the four schemes, with column production rates above 700 km varying by < 30%.

The effect of the reduced H yield in the SR scheme is examined in Figure 4c. The column production rate of H atoms in SR above 700 km is < 25% less than the other three schemes. For the nominal case, H atoms are produced at a rate of 2.16×10^9 cm^{-2} s^{-1} above 700 km. Considering that the eddy mixing time constant is of the same order as the chemical time constant in this region below the homopause level for H atoms, a small variation in the column production rate has a minimal effect on the distribution of H atoms in the upper atmosphere. In the lower atmosphere (< 300 km), where the H chemical lifetime, owing to three-body chain reactions involving H addition, is 3-5 orders of magnitude smaller than the eddy diffusive time constant, the H production is virtually invariant among the schemes, by virtue of the absence of Lyman α-induced methane photolysis.

The true determination of the impact of different branching ratio schemes on the modeling of the atmosphere of Titan is aided by an examination of density profiles of the major hydrocarbons in the atmosphere. A look at the simplest stable hydrocarbon besides CH_4, acetylene (C_2H_2), shows that there is very little variation in abundances, with the mixing ratios varying by little more than 10% among the four schemes (Figure 5a). This behavior follows for many of the observed hydrocarbons, such as C_2H_4 and C_4H_2, as well as those yet to be observed, e.g., C_4H_4 and C_4H_{10}.

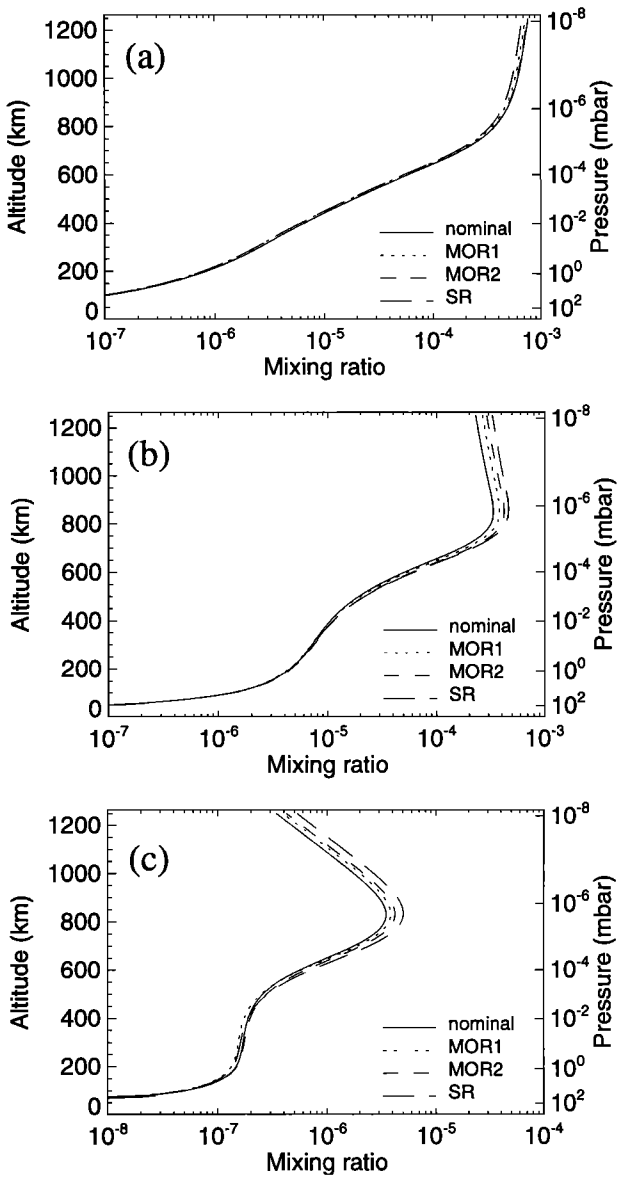

Figure 5. Abundance profiles from the Lyman α-varying schemes for the following constituents: (a) C_2H_2, (b) C_2H_6, and (c) C_3H_8. The solid line denotes the profile for the nominal case, the dotted line denotes MOR1, the short-dashed line denotes MOR2, and the long -dashed line denotes SR.

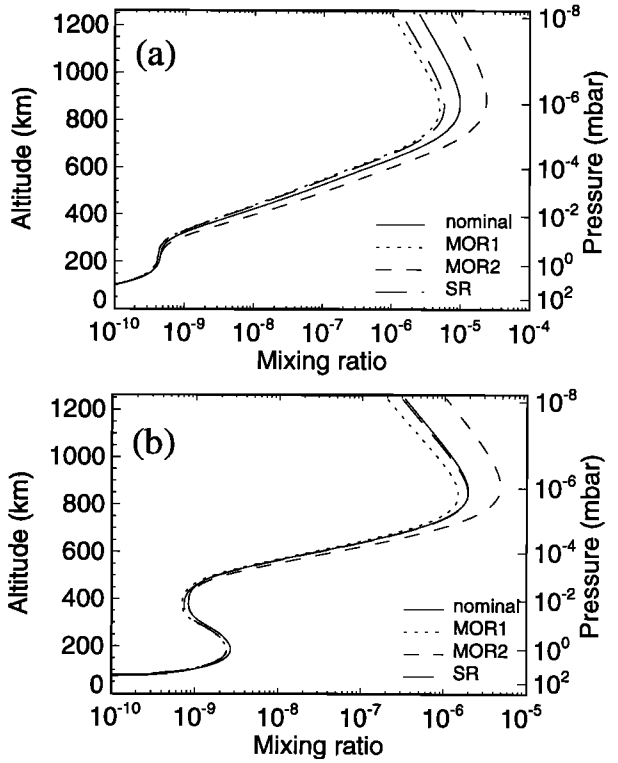

Figure 6. Abundance profiles from the Lyman α-varying schemes for the following constituents: (a) CH_3C_2H and (b) C_3H_6.

However, there are a few hydrocarbons that exhibit a dependence on methane photolysis branching ratios. Figure 5b shows the mixing ratio profile of ethane. The mixing ratio of ethane (C_2H_6) under SR is ~33% greater than the nominal case above 800 km, while it converges below this level. Similarly, in the case of propane (C_3H_8) the SR profile is enhanced over the nominal profile by 30-60% above 800 km (Figure 5c). The methylacetylene (CH_3C_2H) profiles show a larger variation (Figure 6a) with the MOR2 profile, showing an enhancement of > 2 over the nominal profile in the upper atmosphere, while the MOR1 and SR profiles show 70-100% less methylacetylene than the nominal profile. The less abundant allene (CH_2CCH_2) exhibits similar behavior. For propylene (C_3H_6) the nominal profile is ~25% larger than MOR1 at 800 km, increasing to ~60% at 1265 km (Figure 6b). The MOR2 propylene profile, however, is much more enhanced with the MOR2/nominal abundance ratio, increasing to > 2 at 1265 km. For propylene and methylacetylene the greatest divergence from the nominal case occurs with the adoption of the MOR2 scheme. However, MOR2 is a less likely choice for methane photolysis, as mentioned previously.

3.2. Non-Lyman α

We examine the significance of methane product quantum yields at wavelengths other than Lyman α by plotting key molecular production rates and abundance profiles in Figures 7 and 8. Table 3 shows the three schemes we are considering for λ≠Lyman α, with CH_3=1 denoted as P1, $^1CH_2$=0.5, CH_3=0.5 as P2, and $^1CH_2$=1 as P3. Our nominal scheme is assumed for the Lyman α wavelength.

P3 has a $^1CH_2$ column production rate 60% greater than P1 in the Lyman α-influenced region (Figure 7a), displaying the relevance of absorption at all wavelengths in the upper atmosphere. This enhancement is increased between 300 and 650 km, where the $^1CH_2$ column production rate for P3 is 3.5 times larger than that for P1, emphasizing the influence of methane absorption in the middle atmosphere for the $^1CH_2$=1 case. There is no major source of singlet methylene radicals in this region of the atmosphere, other than photolysis, resultant in the mesospheric depletion characterized by P1. The three profiles converge where methane photolysis is negligible for all cases. Compared with $^1CH_2$, the $^3CH_2$ profiles show similar behavior besides the slightly reduced variation in production among the three schemes (Figure 7b) in the upper atmosphere. Because P2 and P3 produce more $^1CH_2$, the diminished influence of quenching in the more rarefied regions of the upper atmosphere affects the more efficient $^1CH_2$-producing schemes more, causing less variation among the three schemes.

As with the Lyman α dependent schemes, CH production is dependent primarily on (R1), and thus the variation among the three schemes for CH production (Figure 8a) follows closely with the variation for $^3CH_2$ production (Figure 7b). Also shown in Figure 8a is the case of the monotonically decreasing CH quantum yield recommended by *Rebbert and Ausloos* [1972/1973], which is shown to be insignificantly different from the P1 case.

CH_3 does not show as much dependence on non-Lyman α methane photolysis as $^{1,3}CH_2$, as shown by the production rate profile (Figure 8b). P1 is enhanced over P3 in the region where methane absorption at wavelengths other than Lyman α is significant. However, below 500 km, production of CH_3 is dominated by the acetylene catalytic scheme (S1) which varies little among the three schemes. Thus, in this region of the

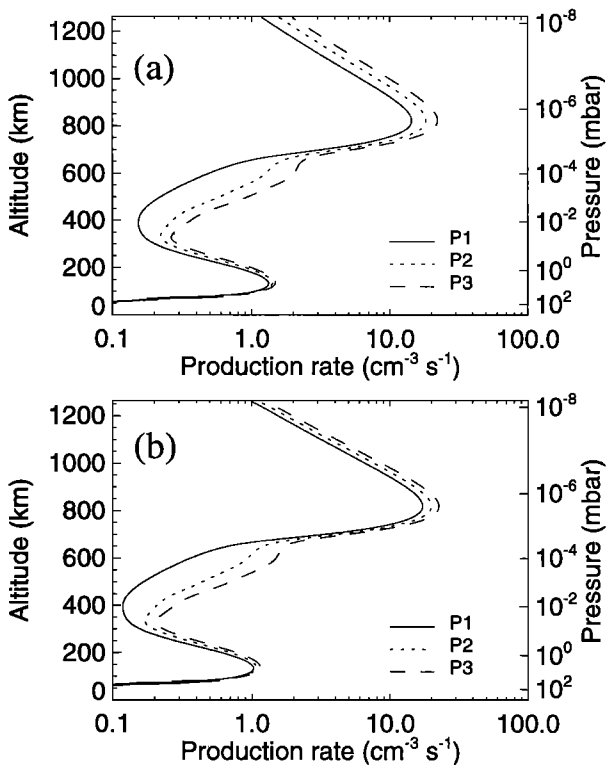

Figure 7. Production rates from the non-Lyman α-varying schemes for CH_2 in the (a) excited state and (b) ground state. The solid line, dotted line, and short-dashed line denote the production rates for P1, P2, and P3, respectively.

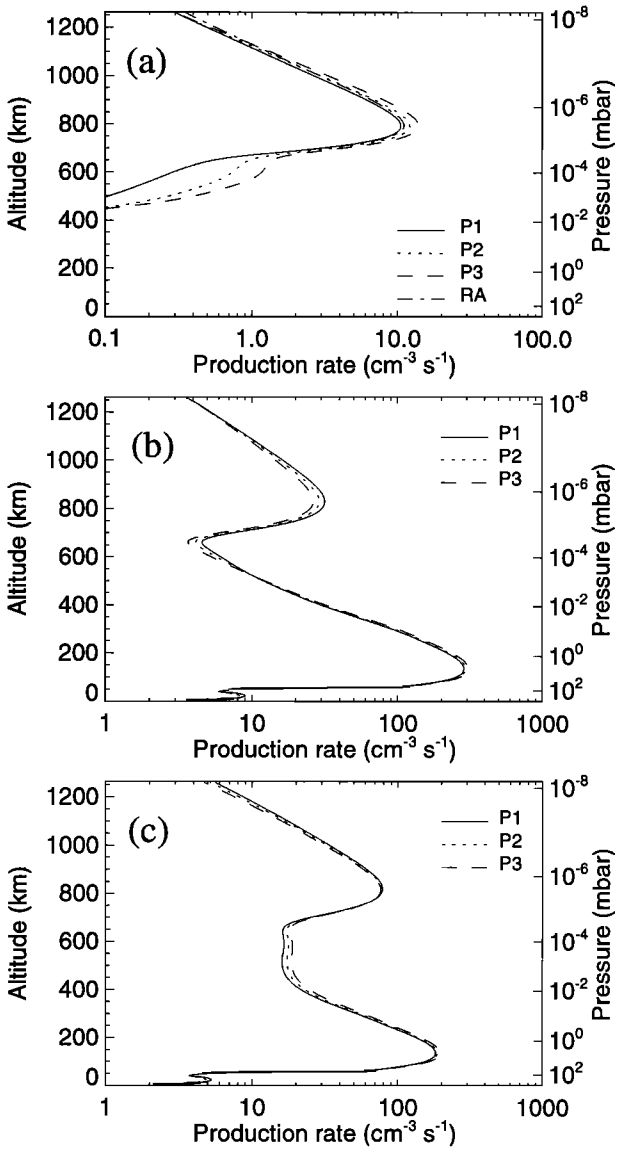

Figure 8. Production rates from the non-Lyman α-varying schemes for the following constituents: (a) CH, (b) CH_3, and (c) H. In Figure 8a, RA denotes the scheme using monotonically decreasing yields for CH from 1048 - 1236 Å in conjunction with *Rebbert and Ausloos* [1972/1973]. The solid line, dotted line, short-dashed line, and dash-dotted line denote the production rates for P1, P2, P3, and RA, respectively.

atmosphere, congruent behavior is exhibited by the three schemes.

The H production rate (Figure 8c) is virtually independent of the quantum yields in question above 625 km, where Lyman α predominates, only showing variation in the middle atmosphere where P3 in enhanced over P1 by a negligible 15%. This fact is contrary to what might be expected, as H atoms are produced by the C-H bond fission process of P1 as opposed to the molecular elimination of P3. In fact, acetylene photolysis is the main source of H atoms in the stratosphere and mesosphere, with the lower peak of H production situated at the level of unit optical depth for C_2H_2 absorption. Acetylene photolysis accounts for 75% of the atomic hydrogen produced below 600 km, and, as will be shown later, C_2H_2 is created through CH and $^{1,3}CH_2$ production. Thus the increase of CH and $^{1,3}CH_2$ production from P3 leads to an enhancement of H production that more than compensates that lack of source from the methane bond fission process characteristic of P3.

As in the Lyman α comparisons, the density profiles for C_2H_2 and many of the other hydrocarbons not presented here show little variation among the three schemes. Figure 9a shows the abundance profiles for ethane. The ethane abundance under the P1 scheme is 65% larger than the P3 profile above 800 km, with the variation decreasing below this altitude. Propane also shows dependence to non-Lyman α quantum yields (Figure 9b) with P1 exceeding P3 by ~50% in the upper atmosphere, while P3 is more enhanced in the stratosphere by only ~20% over P1. The methylacetylene abundance profiles (Figure 9c) show a ~55 % variation in mixing ratio, consistent above 300 km, while converging below this point. For propylene the profiles (Figure 9d) display behavior similar to propane, as P1 is 20% larger than P3 in the upper atmosphere, but in the stratosphere, P3 is enhanced over P1 by ~30% above 150 km.

4. Discussion

Examination of the density profiles of hydrocarbons in Titan's atmosphere clearly reveals that the choice of branching ratio schemes for methane photolysis does not significantly influence all product abundances. Acetylene and ethylene, two important stable hydrocarbons that serve as the basis for the formation of many heavier hydrocarbons, do not show any significant dependence on methane photolysis branching ratios at any wavelength. Ethylene is created in the upper atmosphere through two different addition/elimination mechanisms: radical/radical association,

$$^3CH_2 + CH_3 \rightarrow C_2H_4 + H\,, \qquad \text{(R3)}$$

and the CH-insertion-H-abstraction process involving methane,

$$CH + CH_4 \rightarrow C_2H_4 + H\,. \qquad \text{(R4)}$$

The total production of ethylene among the schemes varies by only 15%, with the proportions of C_2H_4 formation above 600 km by (R3) and (R4) as follows: 56%/42%, nominal; 64%/32%, SR; 68%/29%, MOR1; and 12%/85%, MOR2. Once ethylene is formed, it serves as the major source of acetylene above 500 km through photolysis:

$$C_2H_4 + h\nu \rightarrow C_2H_2 + H_2, 2H\,. \qquad \text{(J6)}$$

This process is responsible for 75% of the total acetylene column production rate above 500 km. Most of this acetylene is diffused

Table 3. Non-Lyman α Methane Photolysis Quantum Yields

Pathways	P1 (nominal)	P2	P3
(J1) $CH_4 + h\nu \rightarrow CH_3 + H$	1.0	0.5	0.0
(J2) $CH_4 + h\nu \rightarrow {}^1CH_2 + H_2$	0.0	0.5	1.0
(J3) $CH_4 + h\nu \rightarrow {}^1CH_2 + 2H$	0.0	0.0	0.0
(J4) $CH_4 + h\nu \rightarrow {}^3CH_2 + 2H$	0.0	0.0	0.0
(J5) $CH_4 + h\nu \rightarrow CH + H_2 + H$	0.0	0.0	0.0

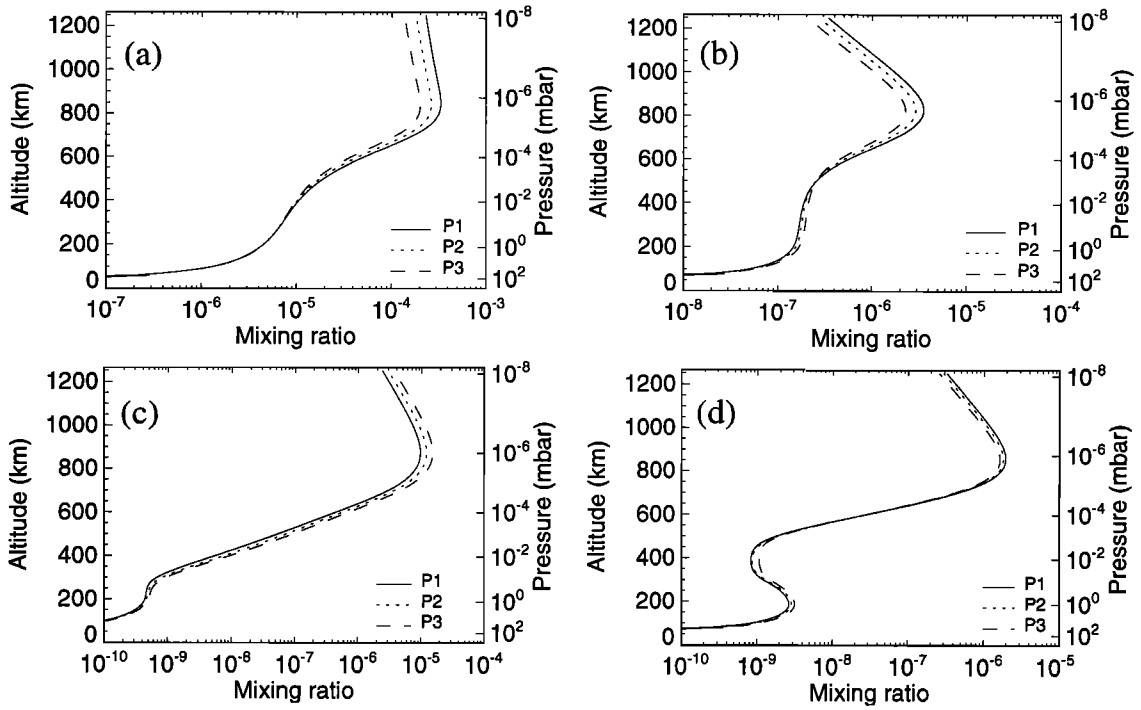

Figure 9. Abundance profiles from the non-Lyman α-varying schemes for the following constituents: (a) C_2H_6, (b) C_3H_8, (c) CH_3C_2H, and (d) C_3H_6.

into the lower atmosphere, where it is recycled through (S1), polymerized to form higher-order hydrocarbons (e.g., C_4H_2),

$$\begin{array}{c} C_2H_2 + h\nu \rightarrow C_2H + H \\ \underline{C_2H + C_2H_2 \rightarrow C_4H_2 + H} \\ 2C_2H_2 \rightarrow C_4H_2 + 2H \end{array}, \quad \text{(S3)}$$

and put through hydrogen chain reactions that serve to reform ethylene:

$$\begin{array}{c} C_2H_2 + H \xrightarrow{M} C_2H_3 \\ \underline{C_2H_3 + H \xrightarrow{M} C_2H_4} \\ C_2H_2 + 2H \rightarrow C_2H_4 \end{array}. \quad \text{(S4)}$$

Thus the equivalence of C_2H_4 formation among the schemes results in the independence of these hydrocarbons from the methane photolysis quantum yield schemes in question.

The production rate profiles that are shown in Figures 2 and 3 indicate that those species whose densities most likely vary according to Lyman α quantum yields are strongly dependent on the production of CH and $^1CH_2$. For example, an important mechanism in producing ethane in the upper atmosphere involves (R2) in the form of

$$\begin{array}{c} CH_4 + h\nu \rightarrow {}^1CH_2 + H_2 \\ CH_4 + {}^1CH_2 \rightarrow CH_3 + CH_3 \\ \underline{CH_3 + CH_3 \xrightarrow{M} C_2H_6} \\ 2CH_4 \rightarrow C_2H_6 + H_2 \end{array}, \quad \text{(S5)}$$

made more meaningful by the large $^1CH_2$-yielding SR scheme. In fact, (S5) produces more than twice the amount of ethane through the SR scheme as through the nominal case. The diminishing influence of Lyman α methane absorption below 800 km, consequently, reduces the variation in ethane density between SR and the nominal profile (Figure 5). Note that the ethane abundance of MOR2 is greater than the nominal profile despite its lack of $^1CH_2$ production. The absence of $^3CH_2$ formation, which accounts for 82% of the total loss of methyl radicals in the upper atmosphere via (R3) for the nominal case, along with the larger methyl yield of MOR2, explains the MOR2 ethane abundance. Clearly, the importance of $^1CH_2$ radicals in ethane production stems from its involvement in producing methyl radicals by (R2). However, the importance of the primary source of methyl radicals is demonstrated in the non-Lyman α comparisons, as the adoption of unit methyl radical yield clearly leads to larger ethane abundances in the methane photolysis region than the $^1CH_2$ case.

Propylene not only has a dependence on $^1CH_2$ production but also maintains a strong dependence on CH radicals in the upper atmosphere. A quick comparison between Figures 6b and 4a shows that the C_3H_6 upper atmospheric density profiles closely follow the CH production rate profiles. C_3H_6 is formed in the upper atmosphere, aided by (S2), (S5), and (R1), through the scheme

$$\begin{array}{c} 2CH_4 \rightarrow C_2H_6 + H_2 \\ CH_4 \rightarrow {}^3CH_2 + 2H \\ {}^3CH_2 + H \rightarrow CH + H_2 \\ \underline{CH + C_2H_6 \rightarrow C_3H_6 + H} \\ 3CH_4 \rightarrow C_3H_6 + 2H_2 + 2H \end{array}. \quad \text{(S6)}$$

The large $^1CH_2$ yield of SR, increasing C_2H_6, results in the SR profile approximating the nominal case, despite its low CH production. The lack of variance of CH yield among the non-

Lyman α-varying schemes produces much less variation among propylene profiles, as shown in Figure 9d.

Likewise, for methylacetylene, the variation in Figure 6a is not displayed in Figure 9c. Methylacetylene is primarily dependent on the production of CH radicals, owing to the lack of variation in ethylene abundance. CH_3C_2H is formed in the upper atmosphere from the direct CH-insertion-H-abstraction process via (R1) and (S2),

$$\begin{aligned} CH_4 &\rightarrow {}^3CH_2 + 2H \\ {}^3CH_2 + H &\rightarrow CH + H_2 \\ CH + C_2H_4 &\rightarrow CH_3C_2H + H \\ \hline CH_4 + C_2H_4 &\rightarrow CH_3C_2H + H_2 + 2H \end{aligned} \quad , \qquad (S7)$$

and indirectly through collisional isomerization of allene,

$$\begin{aligned} CH_4 &\rightarrow {}^3CH_2 + 2H \\ {}^3CH_2 + H &\rightarrow CH + H_2 \\ CH + C_2H_4 &\rightarrow CH_2CCH_2 + H \\ CH_2CCH_2 + H &\rightarrow CH_3C_2H + H \\ \hline CH_4 + C_2H_4 &\rightarrow CH_3C_2H + H_2 + 2H \end{aligned} \qquad (S8)$$

(note that these schemes can also proceed via singlet methylene quenching as demonstrated in (S2)). This dependence on CH radicals is evident as the Lyman α profiles of CH_3C_2H (Figure 6a) mimic the CH production rate profiles (Figure 4a) in the upper atmosphere.

The lack of observations yielding vertical distributions of constituents in Titan's atmosphere makes the modeling of such an atmosphere a wide open affair. The infrared observations [*Coustenis et al.*, 1989; 1991; *Coustenis and Bézard*, 1995; *Kostiuk et al.*, 1997] and ultraviolet observations [*Smith et al.*, 1982] that have been conducted have yielded uncertainties of up to a factor of 2, and we use this value to evaluate the impact of sensitivity of chemical abundances to quantum yield schemes against future Cassini/Huygens observations. The abundance profiles (Figures 4, 5, and 8) indicate that the observed constituents show little or no variation in abundance, among the photolysis schemes, in the stratosphere, where abundances have been observed and dynamical effects play a larger role in determining mixing ratios. For C_2H_6, CH_3C_2H, C_3H_6, and C_3H_8, dependence on Lyman α quantum yields is demonstrated in the upper atmosphere, where a lack of observations persists. However, only the CH-dependent C_3 molecules, CH_3C_2H and C_3H_6, display any variation among the schemes larger than likely observational uncertainty. In varying the non-Lyman α wavelength quantum yields, the dependence is even less potent with the largest variation represented by the 65% enhancement of ethane from P1 over P3, still within likely observational uncertainty.

5. Conclusions

Sensitivity studies regarding the dependence of Titanian hydrocarbon chemistry to methane photolysis quantum yields at wavelengths > 1000 Å have been conducted. We have found that hydrocarbon abundances at altitudes of existing observations are not sensitive to choice of quantum yield scheme, and therefore at the present time, primary quantum yields in methane photolysis cannot be solely used to fit present observations. Furthermore, C_2H_2 and C_2H_4 show no sensitivity to methane photolytic schemes. However, C_3 molecules, such as CH_3C_2H and C_3H_6, exhibit variances that surpass likely observational uncertainty, although the largest variation of these molecules is exhibited by the MOR2 scheme which is highly suspect owing to its very high CH yield. This sensitivity occurs only among Lyman α schemes, and in these cases our nominal scheme provides an intermediate profile among the tested schemes. These results show that differences in constituent abundance profiles among this and other published Titan models [*Yung et al.*, 1984; *Toublanc et al.*, 1995; *Lara et al.*, 1996] (e.g., C_2H_4 abundance profile of Toublanc et al. and Lara et al.) are mainly due to updated chemistry and chosen eddy diffusion profiles, as opposed to methane photolysis scheme.

Smith and Raulin [1999] have suggested a reduced H quantum yield of 0.47 on the basis of the studies of *Heck et al.* [1996] and *Brownsword et al.* [1997b]. We find that the consideration of such an H yield leads to only a 25% reduction in the production of atomic hydrogen at the upper peak of production, compared to the other schemes. Furthermore, in the lower atmosphere, where atomic hydrogen plays a more significant chemical role, the variation among the schemes is virtually nonexistent. Thus we find that a reduced H yield does not significantly affect the subsequent hydrocarbon chemistry.

Although 75% of methane photolysis occurs at Lyman α, knowledge of branching ratios at other wavelengths is significant, as illustrated by the sensitivity manifested by some molecules to choice of photolysis pathway at non-Lyman α wavelengths. In order to fully understand the chemical processes that initiate hydrocarbon chemistry, collision-free studies of methane photolysis at other wavelengths will be necessary for a complete understanding of hydrocarbon chemistry in the atmosphere of Titan. In addition, uncertainty in other atmospheric parameters, such as eddy diffusion, affects the interpretation of the impact of methane photolysis on hydrocarbon chemistry. For instance, we find that the methyl recombination rate, brought into question by the ISO Saturn measurements [*Bézard et al.*, 1998; *Atreya et al.*, 1999], has significant bearing on the effect methane photolysis has on ethane and C_3 molecular abundances. Continued effort in conducting laboratory measurements under conditions applicable to Titan is necessary.

The upcoming Cassini-Huygens mission will not only provide valuable information about the atmosphere of Titan but will also present a view into a natural low-temperature laboratory from which we can examine chemical processes. Upper atmosphere observations of CH-influenced molecules, most notably C_3H_6 and CH_3C_2H, from the Cassini-Huygens mission will provide insight into the nature of the Lyman α photolysis of methane, having implications for the study of other reducing atmospheres in the solar system.

Acknowledgments. This research was supported in part by NASA grants NAG5-4589 and NAG5-8845

References

Aleksandrov, E.N., V.S. Arutyunov, I.V. Dubrovina, and S.N. Kozlov, Study of the reaction of atomic hydrogen with allene, *Kinet. Catal. Engl. Trans.*, *21*, 1323-1326, 1980.

Atreya, S.K., S.G. Edgington, T. Encrenaz, and H. Feuchtgruber, ISO observations of C_2H_2 on Uranus and CH_3 on Saturn: Implications for atmospheric vertical mixing in the Voyager and ISO epochs, and a call for relevant laboratory measurements, *Eur. Space Agency Spec. Publ.*, *ESA SP-427*, 149-152, 1999.

Ausloos, P., R. Gorden Jr., and S.G. Lias, Effect of pressure in the radiolysis and photolysis of methane, *J. Chem. Phys.*, *40*, 1854-1860, 1964.

Baulch, D.L., et al., Evaluated kinetic data for combustion modelling, *J. Phys. Chem. Ref. Data*, *21*, 411-734, 1992.

Bézard, B., H. Feuchtgruber, J. I. Moses, and T. Encrenaz, Detection of methyl radicals (CH_3) on Saturn, *Astron. Astrophys., 334*, L41-L44, 1998.

Bishop, J., P.N. Romani, and S.K. Atreya, Voyager 2 ultraviolet spectrometer solar occultations at Neptune· Photochemical modeling of the 125-165 nm lightcurves, *Planet. Space Sci., 46*, 1-20, 1998.

Bohland, T., F. Temps, and H.G. Wagner, The contribution of intersystem crossing and reaction in the removal of $CH_2(\tilde{a}\ ^1A_1)$ by hydrocarbons studied with the LMR, *Ber. Bunsen-Ges. Phys. Chem., 89*, 1013-1018, 1985.

Braun, W., K.H. Welge, and J. R. McNesby, Flash photolysis of methane in the vacuum ultraviolet, I, End-product analysis, *J. Chem. Phys., 45*, 2650-2656, 1966.

Brownsword, R.A., A. Canosa, B.R. Rowe, I.R. Sims, I.W.M. Smith, D.W.A. Stewart, A.C. Symonds, and D. Travers, Kinetics over a wide range of temperature (13-744 K): Rate constants for the reactions of CH (v=0) with H_2 and D_2 and for the removal of CH (v=1) by H_2 and D_2, *J. Chem. Phys., 106*, 7662-7677, 1997a.

Brownsword, R.A., M. Hillenkamp, T. Laurent, R.K. Vatsa, H.-R. Volpp, and J. Wolfrum, Quantum yield for H atom formation in the methane dissociation after photoexcitation at the Lyman α (121.6 nm) wavelength, *Chem. Phys. Lett., 266*, 259-266, 1997b.

Canosa, A., I.R. Sims, D. Travers, I.W.M. Smith, and B.R. Rowe, Reactions of the methylidine radical with CH_4, C_2H_2, C_2H_4, C_2H_6, and but-1-ene studied between 23 and 295 K with a CRESU apparatus, *Astron. Astrophys., 323*, 644-651, 1997.

Chang, A.H.H., A.M. Mebel, X.M. Yang, S.H. Lin, and Y.T. Lee, Ab initio/RRKM approach toward the understanding of ethylene photodissociation, *J. Chem. Phys., 109*, 2748-2761, 1998.

Chase, Jr., M.W., C.A. Davies, J.R. Downey Jr., D.J. Frurip, R.A. McDonald, and A.N. Syverud, JANAF Thermochemical Tables, 3rd ed., *J. Phys. Chem. Ref. Data Suppl., 14*(1), 1985.

Chastaing, D., P.I. James, I.R. Sims, and I.W.M. Smith, Neutral-neutral reactions at the temperatures of interstellar clouds: Rate coefficients for reactions of C_2H radicals with O_2, C_2H_2, C_2H_4 and C_3H_6 down to 15 K, *Faraday Discuss. Chem. Soc., 109*, 165-181, 1998.

Coustenis, A., and B. Bézard, Titan's atmosphere from Voyager infrared observations, IV, Latitudinal variations of temperature and composition, *Icarus, 115*, 126-140, 1995.

Coustenis, A., B. Bézard, and D. Gautier, Titan's atmosphere from Voyager infrared observations, I, The gas composition of Titan's equatorial region, *Icarus, 80*, 54-76, 1989.

Coustenis, A., B. Bézard, D. Gautier, and A. Marten, Titan's atmosphere from Voyager infrared observations, III, Vertical distribution of hydrocarbons and nitriles near Titan's north pole, *Icarus, 89*, 152-167, 1991.

Edgington, S.G., S.K. Atreya, L.M. Trafton, J.J. Caldwell, R.F. Beebe, A.A. Simon, R.A. West, and C. Barnet, On the latitude variation of ammonia, acetylene, and phosphine altitude profiles on Jupiter from HST Faint Object Spectrograph observations, *Icarus, 133*, 192-209, 1998.

Heck, A.J.R., R.N. Zare, and D.W. Chandler, Photofragment imaging of methane, *J. Chem. Phys., 104*, 4019-4030, 1996.

Kostiuk, T., K. Fast, T.A. Livengood, J. Goldstein, T. Hewagama, D. Buhl, F. Espenak, and K.H. Ro, Ethane abundance on Titan, *Planet. Space Sci., 45*, 931-939, 1997.

Langford, A.O., H. Petek, and C.B. Moore, Collisional removal of $CH_2(^1A_1)$: Absolute rate constants for atomic and molecular collisional partners at 295 K, *J. Chem. Phys., 78*, 6650-6659, 1983.

Lara, L.M., E. Lellouch, J.J. Lopez-Moreno, and R. Rodrigo, Vertical distribution of Titan's atmospheric neutral constituents, *J. Geophys. Res., 101*, 23,261-23,283, 1996.

Laufer, A.H., Kinetics of gas phase reactions of methylene, *Rev. Chem. Intermed., 4*, 225-257, 1981.

Laufer, A.H., and J.R. McNesby, Photolysis of methane at 1236 Å: Quantum yield of hydrogen formation, *J. Chem. Phys., 49*, 2272-2278, 1968.

Lee, L.C., and C.C. Chiang, Photodissociation of CH_4, *J. Chem. Phys., 78*, 688-691, 1983.

Lindal, G.F., G.E. Wood, H.B. Hotz, D.N. Sweetnam, V.R. Eshleman, and G.L. Tyler, The atmosphere of Titan: An analysis of the Voyager 1 radio occultation measurements, *Icarus, 53*, 348-363, 1983.

Magee, E.M., Photolysis of methane by vacuum-ultraviolet light, *J. Chem. Phys., 39*, 855-858, 1963.

Mahan, B.H., and R. Mandal, Vacuum ultraviolet photolysis of methane, *J. Chem. Phys., 37*, 207-211, 1962.

Monks, P.S., F.L. Nesbitt, W.A. Payne, M. Scanlon, L.J. Stief, and D.E. Shallcross, Absolute rate constants and product branching ratios for the reaction between H and C_2H_3 at T=213 and 298 K, *J. Phys. Chem., 99*, 17,151-17,159, 1995.

Mordaunt, D.H., I.R. Lambert, G.P. Morley, N.R. Ashfold, R.N. Dixon, C.M. Western, L. Schnieder, and K.H. Welge, Primary product channels in the photodissociation of methane at 121.6 nm, *J. Chem. Phys., 98*, 2054-2065, 1993.

Mount, G.H., and H.W. Moos, Photoabsorption cross sections of methane and ethane 1380-1600 Å, at T = 295 K and T = 200 K, *Astrophys. J., 224*, L35-L38, 1978.

Mount, G.H., E.S. Warden, and H.W. Moos, Photoabsorption cross sections of methane from 1400 to 1850 Å, *Astrophys. J., 214*, L47-L49, 1977.

Okabe, H., Photochemistry of acetylene at 1470 Å, *J. Chem. Phys., 75*, 2772-2778, 1981.

Okabe, H., Photochemistry of acetylene at 1849 Å, *J. Chem. Phys., 78*, 1312-1317, 1983.

Opansky, B.J., and S.R. Leone, Low-temperature rate coefficients of C_2H with CH_4 and CD_4 from 154 to 359 K, *J. Phys. Chem., 100*, 4888-4892, 1996.

Raulin, F., P. Coll, D. Coscia, M.C. Gazeau, R. Sternberg, P. Bruston, G. Israel, and D. Gautier, An exobiological view of Titan and the Cassini-Huygens mission, *Adv. Space Res., 22*(3), 353-362, 1998.

Rebbert, R.E. and P. Ausloos, Photolysis of methane: Quantum yield of $C(^1D)$ and CH, *J. Photochem., 1*, 171-176, 1972/1973.

Romani, P.N., Recent rate constant and product measurements of the reactions $C_2H_3 + H_2$ and $C_2H_3 + H$ - Importance for the photochemical modeling of hydrocarbons on Jupiter, *Icarus, 122*, 233-241, 1996.

Romani, P.N., J. Bishop, B. Bézard, and S.K. Atreya, Methane photochemistry on Neptune: Ethane and acetylene mixing ratios and haze production, *Icarus, 106*, 442-463, 1993.

Seki, K., and H. Okabe, Photochemistry of acetylene at 193.3 nm, *J. Phys. Chem., 97*, 5284-5290, 1993.

Slagle, I.R., D. Gutman, J.W. Davies, and M. Pilling, Study of the recombination reaction $CH_3 + CH_3 \rightarrow C_2H_6$, I, Experiment, *J. Phys. Chem., 92*, 2455-2462, 1988.

Slanger, T.G., and G. Black, Photodissociative channels at 1216 Å for H_2O, NH_3, and CH_4, *J. Chem. Phys., 77*, 2432-2437, 1982.

Smith, G.R., D.F. Strobel, A.L. Broadfoot, B.R. Sandel, D.E. Shemansky, and J.B. Holdberg, Titan's upper atmosphere: Composition and temperature from the EUV solar occultation results, *J. Geophys. Res., 87*, 1351-1359, 1982.

Smith, N.S., and F. Raulin, Modeling of methane photolysis in the reducing atmospheres of the outer solar system, *J. Geophys. Res., 104*, 1873-1876, 1999.

Strobel, D.F., The photochemistry of hydrocarbons in the Jovian atmosphere, *J. Atmos. Sci., 30*, 489-498, 1973.

Toublanc, D., J.P. Parisot, J. Brillet, D. Gautier, F. Raulin, and C.P. McKay, Photochemical modeling of Titan's atmosphere, *Icarus, 113*, 2-26, 1995.

Tsang, W. and R.F. Hampson, Chemical kinetic data base for combustion chemistry, part 1, Methane and related compounds, *J. Phys. Chem. Ref. Data, 15*, 1087-1279, 1986.

Wagener, R., Influence of temperature on the removal rates of $CH_2(\tilde{a}\ ^1A_1)$ by inert gases and hydrocarbons, *Z. Naturforsch. A*, 45, 649-656, 1990.

Wang, J.-H., and K. Liu, VUV photochemistry of CH_4 and isotopomers, I, Dynamics and dissociation pathway of the H/D-atom elimination channel, *J. Chem. Phys., 109*, 7105-7112, 1998.

Yelle, R.V., D.F. Strobel, E. Lellouch, and D. Gautier, Engineering models for Titan's atmosphere, *Eur. Space Agency Spec. Publ., ESA SP-1177*, 243-256, 1997.

Yung, Y.L., M. Allen, and J.P. Pinto, Photochemistry of the atmosphere of Titan: Comparison between model and observations, *Astrophys. J. Suppl., 55*, 465-506, 1984.

Zabarnick, S., J.W. Fleming, and M.C. Lin, Kinetic study of the reaction $CH(X^2\Pi) + H_2 \leftrightarrow CH_2(X^3B_1) + H$ in the temperature range 372 to 675 K, *J. Chem. Phys., 85*, 4373-4376, 1986.

S.K. Atreya and E.H. Wilson, Department of Atmospheric, Oceanic, and Space Sciences, University of Michigan, Space Research Building, 2455 Hayward, Ann Arbor, MI 48109-2143. (wilson@umich.edu; atreya@umich.edu)

(Received November 24, 1999; revised April 7, 2000;
accepted April 11, 2000.)